Physical Response of the Tropical–Subtropical North Atlantic Ocean to Decadal–Multidecadal Forcing by African Dust

AMATO T. EVAN

Department of Environmental Sciences, University of Virginia, Charlottesville, Virginia

GREGORY R. FOLTZ

NOAA/Atlantic Oceanographic and Meteorological Laboratory, Miami, Florida

DONGXIAO ZHANG

JISAO, University of Washington, and NOAA/Pacific Marine Environmental Laboratory, Seattle, Washington

(Manuscript received 9 August 2011, in final form 19 February 2012)

ABSTRACT

Dust storms are a persistent feature of the tropical North Atlantic and vary over a wide range of temporal scales. While it is well known that mineral aerosols alter the local radiative fluxes, far less is understood about the oceanic response to such forced changes to the radiative budget, particularly on long time scales. This study uses an observation-based climatology of dust surface forcing and an ocean general circulation model to examine the influence of anomalous atmospheric dust cover over the tropical North Atlantic on upper ocean temperature and circulation during 1955–2008. It is found that surface temperature anomalies from the model experiments are forced primarily by local radiation-induced changes to the surface heat budget. The subsurface temperature anomalies are additionally influenced by upper ocean circulation anomalies, which are the response to dust-forced steric changes in dynamic height. The results herein suggest that on decadal time scales dust-forced variability of ocean surface and subsurface temperatures are of a magnitude comparable to observed variability. On longer time scales dust-forced sea surface temperature anomalies vary in phase with the Atlantic multidecadal oscillation, implying that tropical North Atlantic multidecadal variability is related to changes in dust emissions from West Africa.

1. Introduction

Dust outbreaks from West Africa are a persistent feature of the tropical North Atlantic (Kaufman et al. 2005). Estimates of annual emissions of dust range from 170 to 1600 Tg (Engelstaedter et al. 2006), although models may underestimate the actual emissions (Kok 2011). Mineral aerosols have a high single scatter albedo (Myhre et al. 2003) and over dark surfaces the net effect of dust is to displace radiation at the surface to the height of the dust layer (Wong et al. 2009) or the top of the atmosphere (Evan and Mukhopadhyay 2010). Therefore, by bulk formulas, the presence of an elevated aerosol layer over water would tend to cool the ocean.

Schollaert and Merrill (1998) showed a negative correlation between individual dust outbreaks and underlying SST and used a mixed-layer heat budget analysis to suggest that the magnitude of the aerosol direct effect was sufficiently large to force the observed cool anomalies. Evan et al. (2008) demonstrated that on longer time scales such a statistical relationship held, showing that the cross-correlation function of monthly mean SST and dust optical depth anomalies is a maximum when SST lags the dust by one to three months. Foltz and McPhaden (2008a) used satellite and in situ data from the tropical North Atlantic moorings, and a mixed-layer heat budget analysis, to suggest that 35% of the historical (1984–2000) year-to-year changes in summertime SST were radiatively forced by dust. Evan et al. (2008) suggested that

Corresponding author address: Amato T. Evan, Department of Environmental Sciences, University of Virginia, Charlottesville, VA 22904.
E-mail: aevan@virginia.edu

DOI: 10.1175/JCLI-D-11-00438.1

a secular downward trend in dust optical depth from the early 1980s through the early 2000s may have contributed to the upward trend in tropical North Atlantic SST over this same period. Foltz and McPhaden (2008b) used an independent satellite dataset to show that the downward trend in dust, if left unbalanced by other processes, would lead to 3°C increase in the tropical North Atlantic mixed layer temperature. Evan et al. (2009) used a 1D mixed layer model and a highly idealized parameterization of ocean–atmosphere heat fluxes to show that this trend in dust contributed to 20% of the observed upward SST trend, averaged over the region. Lastly, Martínez Avellaneda et al. (2010) used microwave retrieved SST to show that from 2000 to 2006 approximately 30% of SST variability in the eastern tropical–subtropical North Atlantic was forced by dust, with noted individual outbreaks cooling surface temperatures by 0.2°–0.4°C. They also showed that in an ocean general circulation model the climatological SST cooling by dust is approximately 0.5°C.

These empirically based studies all consistently suggest that dust plays an important role in shaping the observed variability of tropical North Atlantic SST. However, results from general circulation model experiments differ in terms of the influence of dust on SST, ranging from virtually no effect (Miller and Tegen 1998) to a mean cooling on the order of 0.5°C (Yoshioka et al. 2007), with discrepancies likely related to dust mass fluxes and aerosol radiative properties (Huneeus et al. 2010). Recently, Mahowald et al. (2010) used an atmospheric general circulation model coupled to a slab ocean to show that the composite difference of annually averaged dust-forced SSTs, for two 10-yr periods of high and low dust concentrations (1955–64 and 1980–89), was 0.1°–0.5°C over the tropical North Atlantic.

Although there have been many recent advances in understanding the influence of African dust outbreaks on tropical North Atlantic SST, one important question that remains unanswered is this: What is the influence of dust on regional SSTs on decadal to multidecadal time scales? Elucidating such physical processes on these long time scales is precisely the focus of this study. The remainder of this manuscript is organized as follows. In section 2 we discuss the physical ocean model used here, including the dust surface forcing climatology, and a validation of the model setup. In section 3 we examine the output of our numerical experiments, focusing on temperature variability of the surface and subsurface, but also considering heat content and velocity anomalies of the upper ocean. We conclude in section 4 with discussion of the results in the context of understanding climate in the tropical North Atlantic.

2. Data and models

In this manuscript we examine the physical response of the upper ocean to variability in aeolian dust on interannual to decadal time scales using a long-term climatology of Atlantic dust radiative forcing at the surface and an ocean general circulation model. The following is a brief discussion of the dust climatology, which is described in more detail in Evan and Mukhopadhyay (2010), and a thorough description of the numerical ocean model we use here.

a. Atlantic dust climatology

Dust surface radiative forcing estimates are from a monthly mean climatology spanning 1955–2008 at a 1° horizontal resolution (Evan and Mukhopadhyay 2010). We refer the reader to Evan and Mukhopadhyay (2010) for an in-depth discussion of the dataset construction, and to Evan et al. (2011) for a comparison to the long-term dataset from Barbados. One limitation of this climatology is that at any location in the tropical Atlantic annual mean dust optical depth is perfectly correlated with dust optical depth at Cape Verde because of the regression model used in the dust reconstruction. Satellite retrievals of annual mean dust aerosol optical depth (DAOD) values across the tropical North Atlantic are highly correlated with DAOD at Cape Verde (Evan and Mukopadhyay 2010), supporting the methodology used to create the long-term climatology. Note, however, that the annual means and standard deviations at any given locations do not necessarily equate, and monthly mean DAOD and the associated radiative forcing are not necessarily correlated with the respective values at Cape Verde.

From this climatology, long-term mean Atlantic DAOD extends westward from the coast of West Africa to the Caribbean and spans the latitudes of 5°–25°N, with the highest concentrations within 8°–18°N and 20°–32°W (Fig. 1). DAOD in the northern tropical Atlantic exhibits a pronounced seasonal cycle; there is a minimum during the November–December period and a maximum during June–July. The summertime maximum in DAOD is more than 3 times the wintertime minimum value (Fig. 2a), consistent with satellite estimates of the DAOD seasonal cycle (Husar et al. 1997; Kaufman et al. 2005). From 1955 to 2008 the annual mean DAOD, averaged over the northern tropical Atlantic (Fig. 2b), is characterized by a peak in dustiness during the mid-1980s, consistent with Prospero and Lamb (2003), and minima in dust cover during the mid-1950s and mid-1960s, consistent with Mahowald et al. (2010), and again during the 2000s, consistent with Evan et al. (2009).

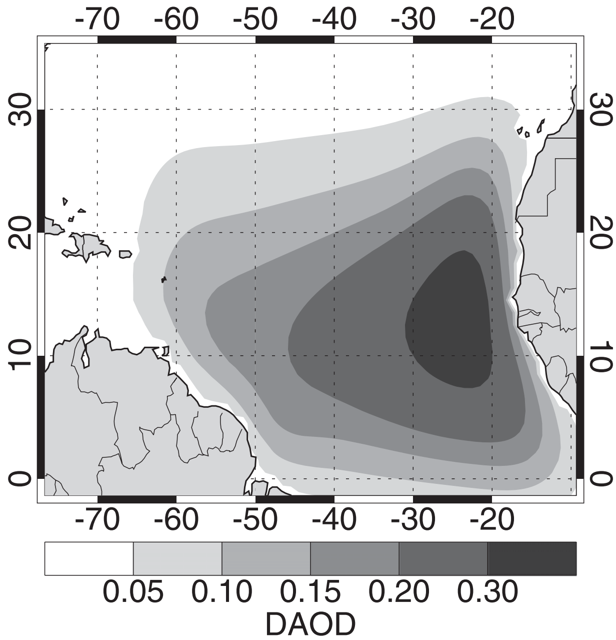

FIG. 1. Long-term mean DAOD over the northern tropical Atlantic. The long-term mean DAOD field is from monthly mean values for the period 1955–2008 and was created with a statistical model to blend recent satellite observations with historical dust proxy data (Evan and Mukhopadhyay 2010).

Dust direct surface radiative forcing closely follows DAOD variability; there is a maximum in the magnitude of the surface forcing in July and a minimum during the boreal fall and winter seasons (Evan and Mukhopadhyay 2010). The range of annual mean surface direct forcing averaged over the northern tropical Atlantic is -5 to -6 W m^{-2}, and monthly mean values range from -3 to -9 W m^{-2} (Evan and Mukhopadhyay 2010). The maximums and minimums in the magnitude of the forcing occur simultaneously with the maximums and minimums in DAOD.

b. *Ocean general circulation model*

We use the Massachusetts Institute of Technology Ocean General Circulation Model (MITgcm) (Adcroft et al. 2002; Marshall et al. 1997a,b) to estimate the physical response of the ocean to dust forcing. The MITgcm is run globally with a horizontal resolution of 1° and 23 vertical layers, with the uppermost layers having a resolution of 10 m and the lower layers becoming coarser with depth to a maximum of 500 m. The bathymetry is from the World Ocean Atlas 2005 (http://www.nodc.noaa.gov/OC5/WOA05/pr_woa05.html; hereafter WOA05) and extends from 80°S to 80°N. The Gent–McWilliams (Gent and McWilliams 1990) eddy parameterization and K-profile parameterization (KPP) vertical mixing scheme (Large et al. 1994) simulate effects of subgrid-scale processes. Surface temperature and salinity are relaxed to a monthly climatology from WOA05 at time scales of two and six months, respectively. Model tracers and momentum have a time step of 240 s.

For model spinup we use climatological monthly surface horizontal momentum fluxes from the National Centers for Environmental Protection (NCEP) Reanalysis I (Kalnay et al. 1996) and climatological monthly surface heat budgets that are calculated offline using surface fluxes of long and shortwave radiation and sensible and latent heat from the NCEP–National Center for Atmospheric (NCAR) Research Reanalysis 1 (NNRP). The model is spun up to steady state in the upper ocean for 100 years using a momentum time step of 240 s and a tracer time step of 6 h. The model is run for an additional 30 yr with momentum and tracer time steps set to 240 s.

During the model spinup and the numerical experiments, model SST and sea surface salinity (SSS) are relaxed to observations. SST relaxation is analogous to a parameterization of the turbulent fluxes of latent and sensible heat, which act to dampen an SST anomaly (e.g., Deser et al. 2003; Evan et al. 2009). SST relaxation in the context of dampening SST anomalies is later examined in detail by considering changes in SST due to radiative forcing by stratospheric aerosols from two major volcanic eruptions. SST relaxation is achieved by modifying the surface heat budget in order to linearly

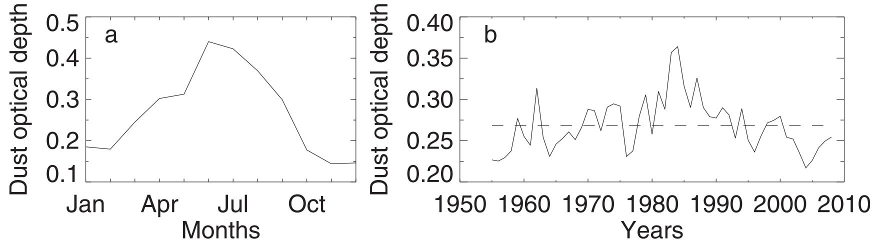

FIG. 2. Seasonal cycle and annual mean time series of DAOD over the tropical northern Atlantic. (a) Monthly climatological and (b) annually averaged DAOD values are based on data covering the 1955–2008 time period and are averaged over the region 10°–20°N, 20°–50°W. The dashed line in (b) represents the long-term mean for this region.

relax the model SST to observed values over the designated relaxation time; that is,

$$H^*_{\rm flux} = H_{\rm flux} + \rho c_p \Delta h \frac{({\rm SST}_M - {\rm SST}_O)}{t_{\rm relax}}, \qquad (1)$$

where $H_{\rm flux}$ is the reanalysis surface heat flux, ρ is the density, c_p is the specific heat of seawater, Δh is the depth of the first model vertical level (10 m), SST_M is the model output SST, SST_O is the observed SST that the model is relaxed to, $t_{\rm relax}$ is the chosen relaxation time, and $H^*_{\rm flux}$ is the resultant surface heat flux required to satisfy (1). Suspended dust cools underlying SST mostly via changes to the surface heat flux, so dust-forced changes to $H_{\rm flux}$ are also damped according to $t_{\rm relax}$, and the magnitude of the response of the upper ocean to dust forcing is sensitive to the choice of $t_{\rm relax}$.

To validate the modeled mean state, we compare the long-term annual mean SST from the World Ocean Atlas (WOA05; Boyer et al. 2005) dataset, which is the SST climatology used for SST_O in Eq. (1), to the model annually averaged SST from the final year of the 130-yr spinup run for $t_{\rm relax}$ of two weeks and two months. For $t_{\rm relax}$ equal to two weeks, the observed and modeled SST climatologies are to large extent in agreement, both having similar meridional SST gradients, cool temperatures along the eastern boundaries in the subtropical regions of the basin, and warm waters coincident with the western boundary currents (Fig. 3). The most obvious difference between the two is that modeled SST in the eastern (western) equatorial Atlantic is warmer (cooler) than in the WOA05 climatology. Here disagreement between the model and WOA05 data is less than 1°C over much of the basin (not shown).

The SST climatology for $t_{\rm relax}$ equal to two months essentially exhibits the same patterns of agreement and disagreement with the WOA05 data, except that here the warm pool in the eastern equatorial region is larger and warmer than in the model climatology with $t_{\rm relax}$ equal to two weeks (Fig. 3). Also, for this longer SST relaxation time it is not clear that the surface waters over the western boundary currents are much warmer than those farther east at the same latitudes. However, despite these differences, disagreement between the model, for $t_{\rm relax}$ equal to two months, and the WOA05 data is less than 2°C over much of the basin (not shown). By (1), when $t_{\rm relax}$ is set to two weeks the model SST will agree better with the observed SST than when compared to modeled SST for $t_{\rm relax}$ set to a longer time scale, so the fact that there is better agreement between the model and observations for $t_{\rm relax}$ set to two weeks is not surprising. At the same time we note a strong similarity between the two model climatologies (Fig. 3).

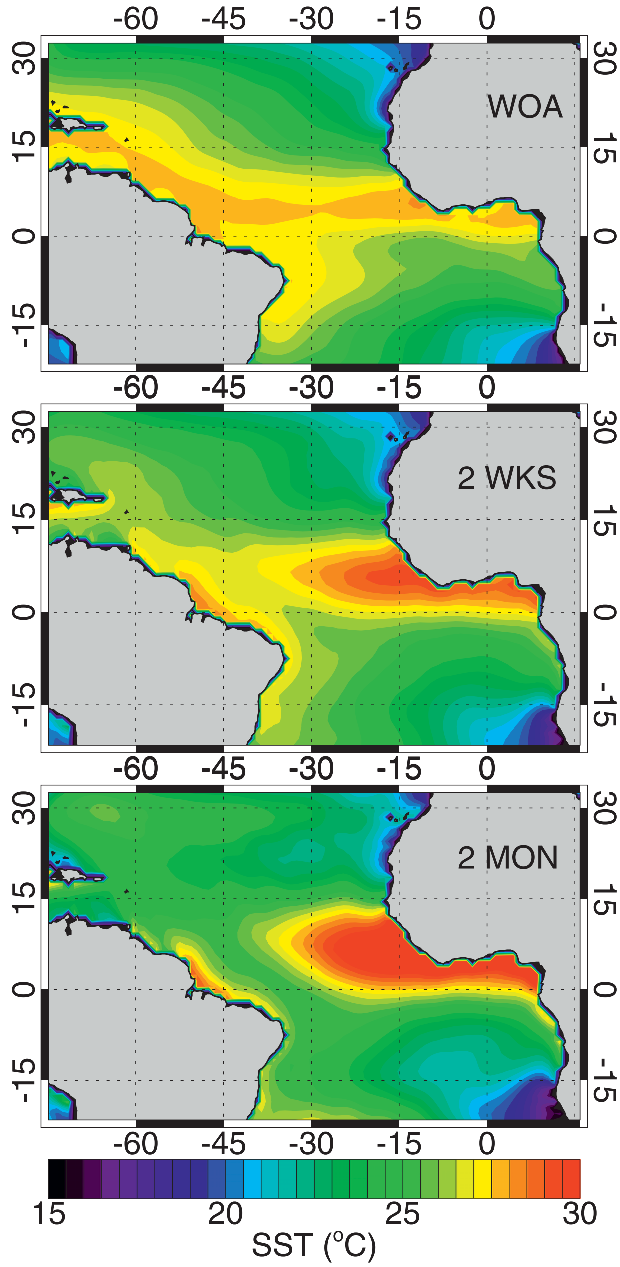

FIG. 3. Comparison of observed and modeled annual mean SST fields. Shown are annually averaged SST from (top) the WOA05 climatology (WOA) and the model output for $t_{\rm relax}$ [Eq. (1)] set to (middle) two weeks (2 WKS) and (bottom) two months (2 MON).

We also compare the observed and modeled climatological SST seasonal cycle by mapping the difference in the mean boreal summer [July–September (JAS)] and winter [February–April (FMA)] SST fields. Model output for $t_{\rm relax}$ of two weeks and two months captures the major features of the seasonal cycle fields, including a very weak seasonal SST difference along the equatorial waters and the western boundaries and a larger seasonal difference in the subtropics and along the eastern boundaries (Fig. 4). Neither model climatology captures the region of a weak SST season cycle from observations that extends south from the equator and is west of 15°W, and both model climatologies have the region of a weak seasonal cycle that extends along the equator as being too narrow when compared to the WOA05 data. In addition, for t_{relax} equal to two months, to the north of the 30°N latitude the model produces a seasonal cycle that is much stronger than that from the WOA05 data. Despite these differences, over much of the tropical North Atlantic the differences between the modeled and observed SST annual cycle for each model configuration are on the order of 1°C or less.

We examined the influence of t_{relax} on the modeled SST response to surface radiative forcing from the eruptions of El Chichón (1982) and Mount Pinatubo (1991). After each eruption elevated levels of stratospheric aerosols greatly reduced the surface solar insolation, cooling surface and subsurface temperatures globally. The SST response to each eruption is unique to other forms of internally and externally forced variability and therefore it is possible to isolate the volcanic signal in observed SST. To do so we create a monthly time series of observed SST using the data from the Hadley Centre Global Sea Ice and Sea Surface Temperature (HADISST 1.1) dataset (Rayner et al. 2003). We create a time series of monthly mean HADISST SST from 1980–2000 that is averaged over the northern tropical Atlantic (0°–30°N, 20°–65°W). The time series' annual cycle is removed by subtracting the climatological monthly mean from every monthly mean SST value. Finally, the time series is detrended to remove variability associated with greenhouse gas forcing or other secular processes.

To quantify the magnitude of the aerosol-forced changes to the HADISST SST time series, SST anomalies must be defined as relative to a mean over some period. Following the methodology of Santer et al. (2001) we define anomalies relative to the mean SST for the 1-, 2-, and 3-yr periods preceding the 1982 eruption of El Chichón (Fig. 5). The resulting SST anomaly time series exhibits cool anomalies on the order of 0.5°C in the year following the eruptions of El Chichón and Mount Pinatubo (Fig. 5), consistent with other studies (Evan et al. 2009; Santer et al. 2001).

We model the response of SSTs to these eruptions for t_{relax} values of two weeks, one month, and two months (Fig. 5). SST forcing by stratospheric aerosols is determined by differencing the output of a control run from a perturbed run. The control run is forced by seasonally varying reanalysis surface heat fluxes and horizontal wind stress for a 23-yr period. The perturbed run

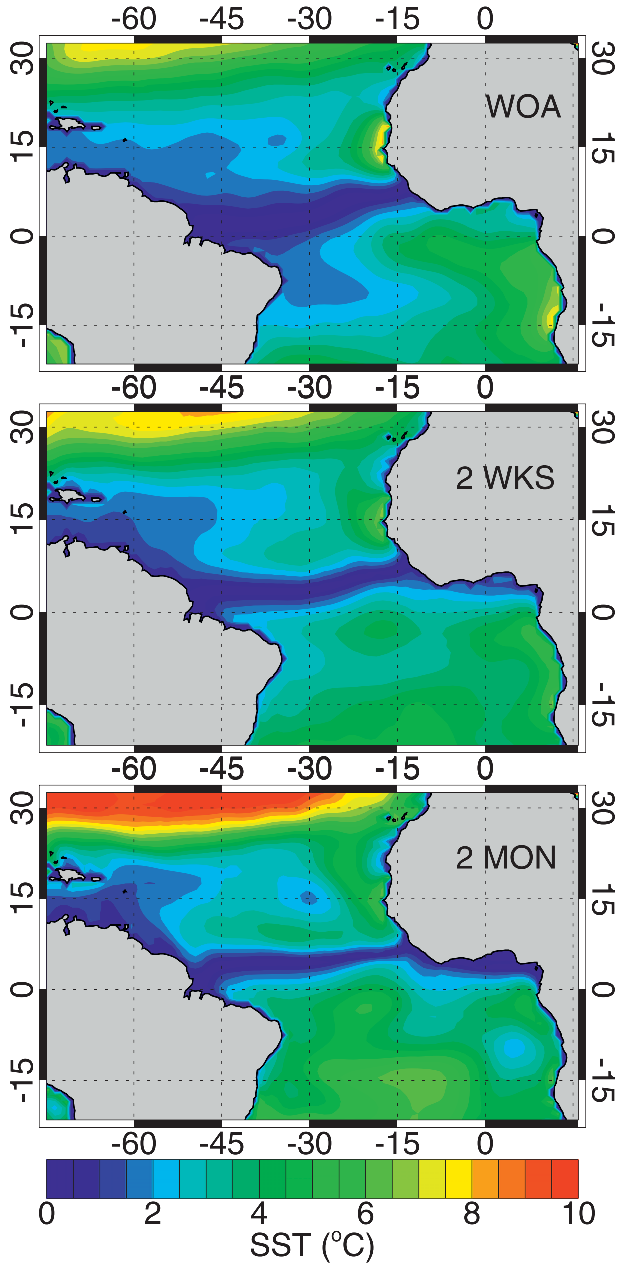

FIG. 4. Comparison of observed and modeled annual cycle magnitude. Shown are the mean boreal summer (JAS) and winter (FMA) SST from (top) the WOA05 climatology (WOA) and the model output for t_{relax} [Eq. (1)] set to (middle) two weeks (2 WKS) and (bottom) two months (2 MON).

is forced by the same seasonally varying surface fluxes of heat and momentum, but the heat flux is also modified to account for changes in downwelling radiative fluxes due to the buildup and decay of stratospheric aerosols from the eruptions. Estimates of the volcanic aerosol radiative forcing at the surface are from Evan et al. (2009). We define the modeled influence of volcanic eruptions

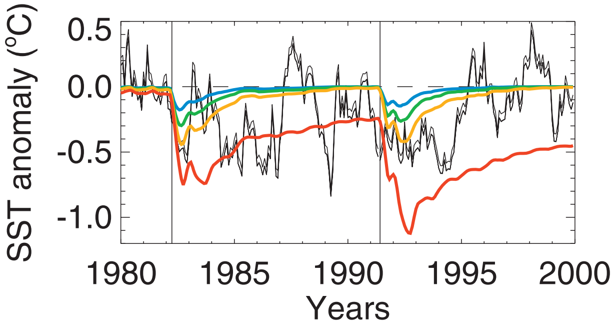

FIG. 5. Observed and modeled tropical North Atlantic SST anomalies following the eruptions of El Chichón (1982) and Mount Pinatubo (1991). Plotted are three monthly mean SST anomaly time series (black) from observations (HADISST2) in which the time period used to calculate the mean is different for each (see text). Also shown is the modeled response to the volcanic eruptions for an SST relaxation time scale, t_{relax} [Eq. (1)], of two weeks (blue), one month (green), and two months (orange), and for the relaxation turned off (red). All time series are averaged over 0°–30°N and 20°–65°W and the vertical lines indicate the time of each major eruption.

on tropical North Atlantic SST as the SST from the perturbed run minus the control run SST. We construct the monthly mean time series of modeled SST over the same domain as that for the observations.

The sensitivity of modeled SST to the eruptions grows progressively larger as t_{relax} varies from two weeks to two months (blue, green, and orange lines in Fig. 5). Model SST anomalies appear to underestimate the influence of stratospheric aerosols for t_{relax} of two weeks, evidenced by a maximum anomaly magnitude less than 0.2°C after each eruption, accounting for only one-third of the observed cooling. Model SST anomalies for t_{relax} of one month better reproduce the large peak in cooling that follows each eruption, but still are only able to account for half of the observed cooling. Model SST anomalies for t_{relax} of two months appear to do a good job of representing the dramatic cooling observed in the one to two years following each eruption, given the excellent agreement with the observations. The progressively weaker SST response to the aerosol forcing with the shortening of the relaxation time scale is analogous to a reduction in the time scale over which SST anomalies are damped to the atmosphere by turbulent fluxes of latent and sensible heat. Evan et al. (2009) empirically derived an SST relaxation time scale of approximately two months for most of the tropical North Atlantic, consistent with these results.

To illustrate the importance of SST relaxation in such model environments we conducted an additional experiment for which the relaxation was turned off (i.e., t_{relax} is infinity). Here, for the 23-yr control and perturbed runs we replace H_{flux} (from NNRP) with the H^*_{flux} that was calculated within the 23-yr control run for which t_{relax} was set to two weeks. We then turn off SST relaxation in the model. In the control run the climatological fields of long-term mean SST and the SST annual cycle are identical to those shown for t_{relax} equal to two weeks (Figs. 3 and 4). However, as there are no additional heat fluxes into the ocean to compensate for the cool SST anomalies that follow each eruption, with no relaxation the modeled SST anomalies are very large and decay on unrealistically long time scales (red line, Fig. 5). These results imply that turning off SST relaxation in the model will lead to an overestimation of forced SST anomalies. Although model t_{relax} of two months is slightly less effective at reproducing climatological SST fields (Figs. 3 and 4), t_{relax} of two weeks to one month likely underestimates the magnitude of forced SST anomalies (Fig. 5). We therefore utilize a model relaxation time scale of two months for the remainder of this study.

Finally, at both SST relaxation time scales, the model reproduces reasonably well the major circulation features of the tropical and subtropical Atlantic, comparable to other coarse resolution models used in climate study, including the western boundary currents, the equatorial currents, and the dominant features of the subtropical gyres (not shown). Anomalies of ocean currents associated with the dust forcing will be reported later.

3. Numerical experiment results

As previously noted, we use a dust surface forcing climatology from Evan and Mukhopadhyay (2010) in order to estimate the physical response of the ocean to variability in atmospheric dust. We perform model control and perturbed runs, each initialized from the 130-yr spinup described in section 2 and set up in a manner similar to the previously described numerical experiments that were used to estimate the effect of volcanic eruptions on SST. In the control run we integrate forward an additional 54 yr (1955–2008) from the end of the spinup run, using the same seasonally varying monthly surface forcing (H_{flux}). For the perturbed run we add to the seasonal surface heat fluxes a radiative forcing contribution from anomalous DAOD. The dust-forced contribution to the surface heat flux is defined as the anomalous dust aerosol direct effect at the surface (i.e., we removed both the long-term mean and the mean seasonal cycle from the dust forcing climatology). Here we are relying on the fact that the model already reproduces the correct SST mean state via H^*_{flux} [Eq. (1); Figs. 3 and 4).

The difference between the control and perturbed runs is interpreted as the effect of departures in dustiness from the seasonal mean on the physical state of the

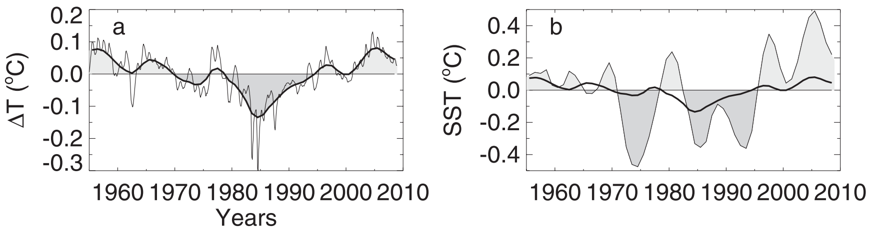

FIG. 6. Annual mean time series of ΔT and observed SST for 1955–2008. All time series are from monthly mean fields averaged over the region 12.5°–20°N, 20°–50°W. The shaded areas represent warm (light gray) and cool (dark gray) (a) annual mean ΔT and (b) observed SST (shaded region encompassing the thin black line) anomalies that have been smoother with a 5-yr low-pass filter. The thin black line overlying the observed SST anomalies in (b) is the same time series shown in (a) (thick line).

ocean. We note that the approximately linear scaling of the volcanic aerosol-forced SST anomalies with changes in the SST relaxation time scale (Fig. 5) was also apparent when estimating the dust-forced SST anomalies in the tropical North Atlantic for model experiments when t_{relax} was set to two weeks and two months (not shown). As we are modeling the effect of departures in dustiness from the seasonal mean state, the long-term mean dust radiatively forced change in SST (hereafter referred to as ΔT) is everywhere on the order of 0.001°C.

a. Time series of ΔT

From 1955–2008 monthly mean ΔT averaged over 12.5°–25°N and 20°–60°W has a range of 0.43°C, with the warmest anomalies occurring in the beginning and end of the half-century record, and cool anomalies in the middle of the time series (Fig. 6a). A 5-yr low pass filtered annual mean time series of ΔT (via two recursive 3-yr running mean filters) highlights coherent periods of warm and cool anomalies, including warm anomalies from the beginning of the record to 1970, a cool period from 1970 through 1976 that is followed by a brief warm anomaly of 3 yr, a 15-yr cool anomaly from 1979 through 1994, and a 14-yr warm anomaly from 1995 through the end of the record (Fig. 5a). Warming from anomalously low dust cover during the late 1950s and cooling from the more intense and persistent dust cover of the 1980s were noted by Mahowald et al. (2010). The cool period of the 1980s and the transition from a minimum in 1985 to a maximum in the mid-2000s have been noted by Evan et al. (2009) and Foltz and McPhaden (2008b).

Within this same region 5-yr low-pass filtered observed SST anomalies (from HADISST1) exhibit a range of 1.0°C and also show coherent periods of cool and warm anomalies (Fig. 6b) that are both internally and externally forced (Trenberth and Shea 2006; Evan et al. 2009). The observed period of cool and warm SST anomalies match the anomalous periods of ΔT. For example, there are warm anomalies in each time series from 1995 onward, and both show the magnitude of this anomaly being near zero during 2000. Likewise, observed warm SST anomalies from 1970 through 1995 tend to match those in the ΔT series. The observed cool anomaly from 1982 to 1995 is preceded by the cool dust-forced anomaly starting in 1979. This coherence in anomalies suggests that changes in dust cover may be forced by processes associated with SST variability (Wong et al. 2008), that changes in SST are simultaneously affecting African rainfall and thus dustiness (Prospero and Lamb 2003; Giannini et al. 2003; Foltz and McPhaden 2008b), that there is a coupled equatorial response to the dust forced SST anomalies (Evan et al. 2011), or that a combination of the three processes is at play.

The ΔT time series also shows possible multidecadal-scale variability. A 15-yr low-pass filtered ΔT time series (via a 13-point triangle filter) exhibits warm anomalies from 1955 to 1970 (15 yr), cool anomalies from 1970 to 1995 (25 yr), and again warm anomalies from 1995 to 2008 (13 yr) (gray line, Fig. 7). Although there are not enough data to detect a robust multidecadal signal in SST that is forced by dust, the results do indicate that

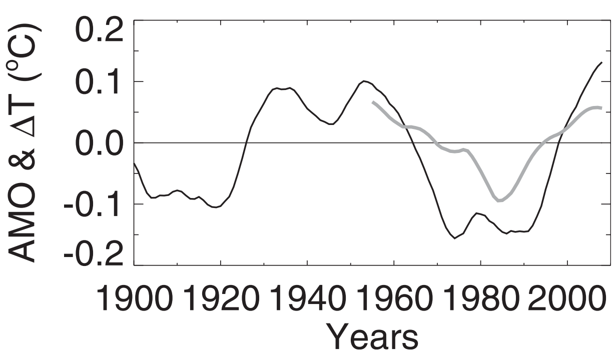

FIG. 7. Time series of the AMO and smoothed ΔT. The AMO time series (black line) is constructed in a manner consistent with Trenberth and Shea (2006) and the ΔT series (gray) is averaged over the region 12.5°–20°N, 20°–50°W and has been smoothed with a 15-yr low-pass filter.

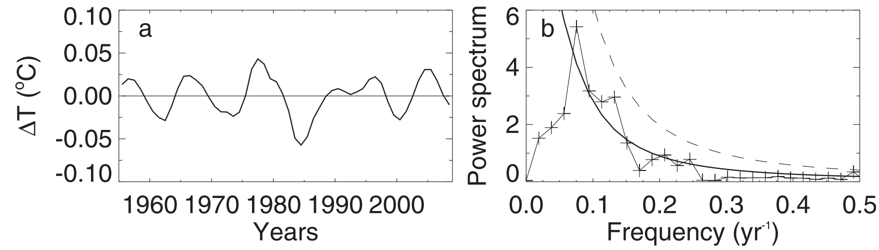

FIG. 8. Bandpass filtered (decadal) ΔT time series and frequency power spectrum. (a) The time series of ΔT is averaged over 12.5°–20°N, 20°–50°W and has been filtered with a 10-yr bandpass filter (see text). (b) The associated FFT power spectrum shows the ΔT spectral peaks (black line with crosses) an equivalent red noise spectrum (thick black line), and the 95% significance level for the spectra (dashed line).

any such oscillation would have a period and amplitude on the order of 50 yr and 0.1°C, respectively. This low-frequency ΔT variability during 1955–2008 is in phase with the Atlantic multidecadal oscillation (AMO; Trenberth and Shea 2006; black line, Fig. 7) and has approximately half the amplitude of the AMO, further suggesting the possibility of positive coupled feedbacks among SST, Sahel rainfall, and African dust on multidecadal time scales (e.g., Evan et al. 2011).

We examine decadal-scale variability of ΔT by subtracting from the 5-yr smoothed annual time series (Fig. 6a) a ΔT time series that has been smoothed with two recursive 17-yr running mean filters that include the series endpoints, qualitatively similar to removing the downward linear trend in the data from the beginning of the series to the peak in the cool anomaly (1985) and the upward linear trend from 1985 through 2008. A longer time series for which a more formal analysis of decadal-scale variability could be evaluated for significance would warrant more careful smoothing, but for our illustrative purposes this approach is sufficient.

Except for the anomalous cool period that persists from 1980 to 1990, this bandpass filtered time series of ΔT exhibits regular decadal-scale variability with an amplitude of 0.05°C (Fig. 8a), which is one-half the magnitude of the 5-yr smoothed ΔT anomalies shown in Fig. 6a. Cool anomalies are observed during the first half and warm anomalies are observed during the second half of each decade (Fig. 8a). A Fourier transform of the bandpass filtered ΔT time series shows spectral peaks that are greater in magnitude than a red noise spectrum (based on the 1-lag autocorrelation of the filtered ΔT time series) at periods of 7–13 years (Fig. 8b). We note that because of the short length of the ΔT time series none of the spectral peaks are determined to be above the 95% significance level (dashed line, Fig. 8b), but our results do suggest a need for development and analysis of longer dust proxy records to further elucidate such dust-forced decadal SST variability of the tropical North Atlantic.

b. *Spatial structure of dust-forced changes to SST, velocity, and heat content*

Having considered changes in dust-forced SST anomalies averaged over a subset of the tropical North Atlantic during 1955–2008 we next examine the spatial structure of the upper ocean response to dust variability and consider the governing physical processes. As previously discussed we model the effect of anomalous dust

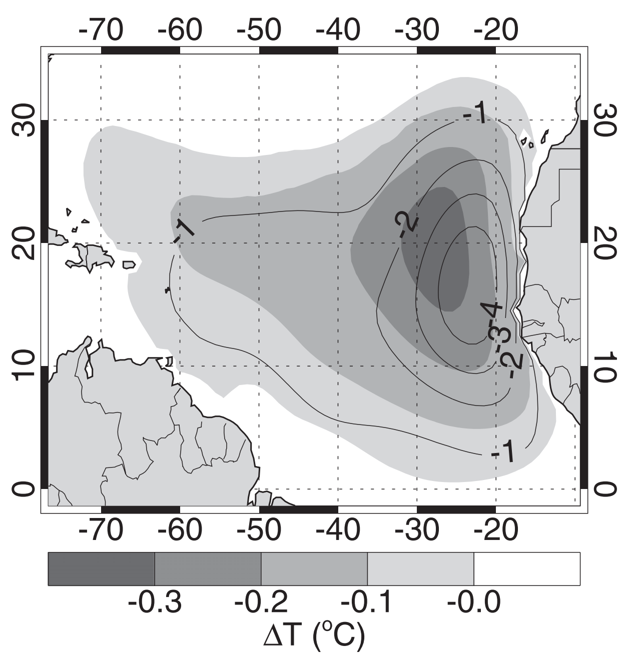

FIG. 9. Composite maps of ΔT and ΔF. Composite differences of ΔT (shading, °C) and all-sky dust surface forcing (ΔF, contours, W m^{-2}) are defined as the difference between the anomalies of the respective variables averaged over the 5 yr of minimum (1983–88) and maximum (1955–57, 2004, 2005) tropical North Atlantic ΔT anomalies (Fig. 6a).

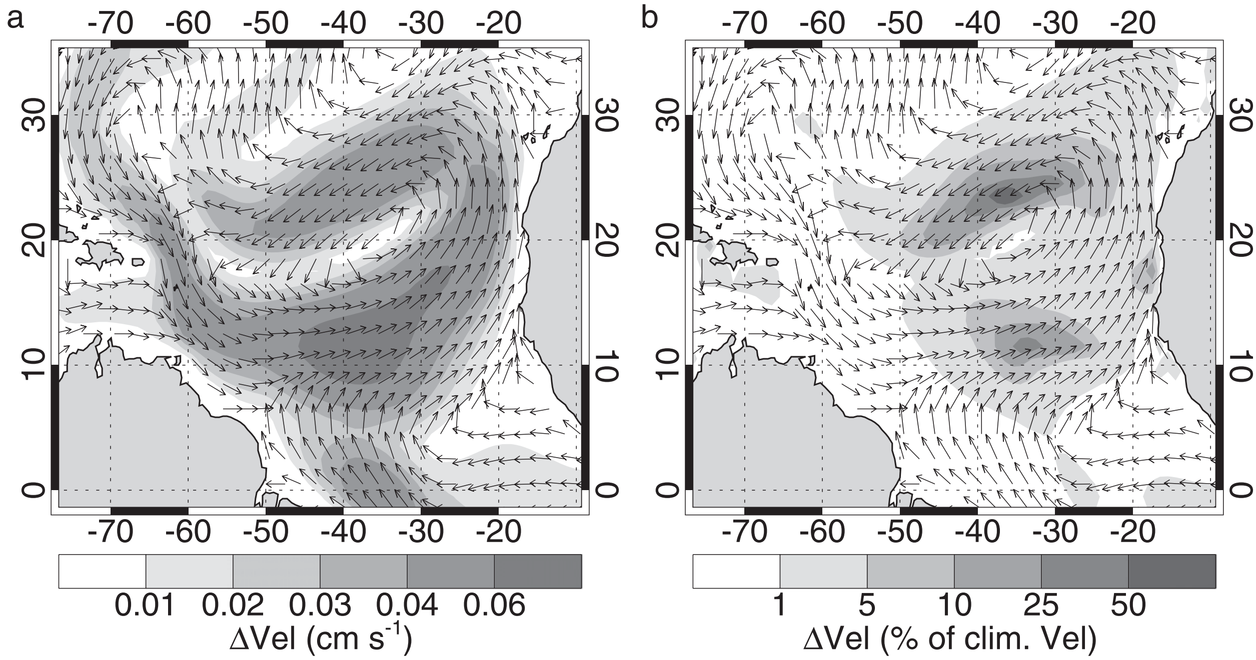

FIG. 10. Composites of upper ocean velocity and velocity as a fraction of the mean current magnitude. Contours are constructed as described in Fig. 9. Arrows are unit length and indicate direction of the anomalous current only. Shading represents (a) the magnitude of the circulation average or (b) the magnitude of the anomalous circulation as a percent of the climatological (model) current magnitude.

surface forcing, and therefore the long-term mean of the perturbed model run is nearly equal to the long-term mean of the control run, and at the surface these differences are everywhere on the order of 0.001°C. To examine the spatial structure of the effect of anomalous dustiness on the upper ocean we instead quantify the effect of dust variability on the state of the upper ocean by differencing composites of the five years for which annually averaged ΔT, averaged over the tropical North Atlantic (Fig. 6a), was the most negative (1983–88) and the most positive (1956–58, 2004, 2005).

A composite difference map of ΔT (hereafter referred to as ΔT_c) is similar in structure to the DAOD climatology (Fig. 1), with a maximum difference between $-0.3°$ and $-0.4°C$ over the region 15°–24°N and 23°–32°W (shaded contours, Fig. 9). To the west the gradient of ΔT_c is weaker than to the north or south, consistent with the spatial structure of the climatological dust optical depth (Fig. 1), and this westward extension of ΔT_c follows the southern branch of the subtropical gyre. We note that the spatial structure of similarly constructed ΔT anomalies from a recent coupled GCM study (Mahowald et al. 2010) are more equatorward than those reported here.

We also show a composite map of all-sky dust forcing (hereafter referred to as ΔF_c), constructed from the dust forcing climatology used in the perturbed run (Fig. 9, contours). Note that ΔF_c and ΔT_c have a qualitatively similar spatial structure, although internal ocean processes shift the maximum (in magnitude) of the cooling to the northwest of the forcing maximum (in magnitude) by approximately 1000 km. Despite this, for the regions where ΔT_c values are less than -0.05, the spatial patterns of ΔT_c and ΔF_c are correlated with an r value of 0.8.

A 5-yr composite difference of ocean currents averaged over the top 100 m of the model (hereafter referred to as ΔVel) shows an anomalous cyclonic circulation that opposes the subtropical gyre (Fig. 10a). This anomalous circulation is the geostrophic adjustment to the cool temperature anomalies (Fig. 9) that extend below the surface (discussed further in section 3d). Note that ΔVel also exhibits a cross-equatorial flow from the southern to the Northern Hemisphere near the Brazilian coast that is coincident with the North Brazil Current. Between approximately 60° and 75°W ΔVel flows southward, in opposition to the Gulf Stream and the Caribbean currents, and breaks eastward near 15°N, following the North Equatorial Current.

The magnitude of ΔVel is small, less than 0.1 cm s^{-1} (Fig. 10a). However, except for the western boundary currents, the model's climatological current speeds in the region of the dust-forced circulations are also small, everywhere less than 3 cm s^{-1} and in many areas less than 1 cm s^{-1} (not shown). Thus, in some places the magnitude of the dust-forced changes in ΔVel represents a significant portion of the climatological currents. For example, in the region of 10°–30°N and 25°–45°W the magnitude of ΔVel is 5%–50% of the climatological current speed (Fig. 9b). Therefore, it is plausible that anomalous dust cover plays a nonnegligible role in altering ocean circulation over the eastern sector of the tropical North Atlantic.

The northward branch of the anomalous cyclonic circulation (Fig. 10a) advects warm water northward by acting on the positive climatological meridional SST gradient (Fig. 3) and thus may explain why the ΔT_c maximum is offset to the northwest of the ΔF_c maximum (Fig. 9). Similarly, the southward branch of the anomalous circulation that overlays the Gulf Stream is advecting cool water equatorward, possibly explaining the nonzero ΔT_c values that lie well to the northwest of the -1 W m^{-2} ΔF_c contour (Fig. 9). This noted importance of advection in shaping temperature anomalies in the region of 10°–20°N latitude is consistent with the surface heat budget analysis of Foltz and McPhaden (2006).

The relationship between ΔVel and dust-forced changes in the upper ocean temperature is elucidated by examining composites of upper ocean streamlines (ΔΨ) and upper ocean heat content (ΔUOHC). Not surprisingly, ΔΨ contours largely follow those from ΔUOHC and the spacing of the ΔΨ contours are closest where the ΔUOHC values are the largest in magnitude (Fig. 11), suggesting that the ΔVel circulation (Fig. 10) is a response to steric changes caused by the cool ΔT_c values (Fig. 9). The maximum (in magnitude) ΔUOHC values are between -30 and -20 kJ cm^{-2}, found in a region centered on 30°W and 20°N. The contours of ΔUOHC stretch southwestward from this maximum, following ΔVel, and extending to 50°W and 15°N ΔUOHC values are greater (in magnitude) than -10 kJ cm^{-2}. The -5 kJ cm^{-2} contour extends northward from the western boundary to 35°N, and the -2 kJ cm^{-2} contour nearly reaches the 45°N latitude (not shown). The ΔUOHC contours cross the ΔT_c contours (Fig. 9), suggesting that the response of the subsurface water is not solely forced by changes to the surface heat flux, but that internal processes are also of importance.

We also examined northward volume transport integrated across 20°N in the model output. The northward transport varied in phase with the dust anomalies, although the magnitude of the anomalies was an order of magnitude smaller than observed decadal variability. The anomalies were on the order of -0.02 Sv (1 Sv $\equiv$ 10^6 m^3 s^{-1}) during those periods when dust was low (e.g., 1950s, 2000s), and 0.025 Sv during the peak in dustiness of the 1980s (not shown).

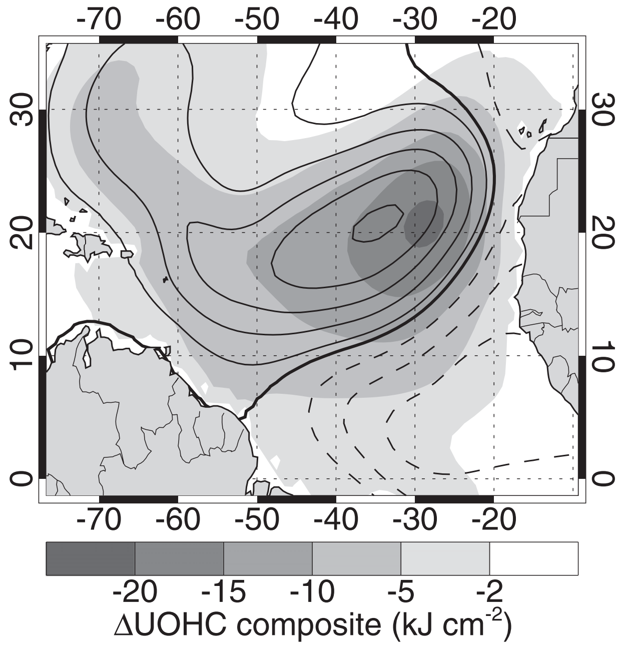

FIG. 11. The ΔΨ and ΔUOHC composite map. Description of composites is as in Fig. 9. The ΔΨ contours are from the nondivergent part of the ΔVel composites (Fig. 10) and suggest anomalous circulations that govern the displacement of ΔUOHC anomalies away from the region of direct surface forcing (Fig. 9). Positive (negative) streamfunction contours indicate counterclockwise (clockwise) rotation, and the distance between contours indicates the magnitude of the anomalous circulation.

c. Evolution of subsurface temperature anomalies

Time series and composite differences of SST, upper ocean currents, and UOHC suggest that Atlantic dust cover variability alters the physical structure of the tropical North Atlantic on interannual to possibly multidecadal time scales. It is therefore constructive to consider the time evolution of the dust-forced temperature anomalies at depth. To do so we examine transects of dust-forced changes in potential temperature (hereafter Δθ) along 20°N over a 1-yr period during which DAOD values were the highest on record. Here we estimate the base of the mixed layer (ML) using the 0.125σ criteria (de Boyer Montégut et al. 2004), based on the model output for the perturbed run only.

During 1983 anomalously strong and persistent dust activity forced cool ΔT anomalies over the tropical northern Atlantic (Fig. 6a). In January 1984, as the winter ML deepens the cool Δθ anomalies are mixed down to the base of the wintertime ML, which we calculate as being 60–70 m (Fig. 12). In March, as the ML begins to shoal, the cool Δθ anomalies that were mixed down during the winter months remain at depth, which is below the base of the March ML. In May the ML is approaching the annual

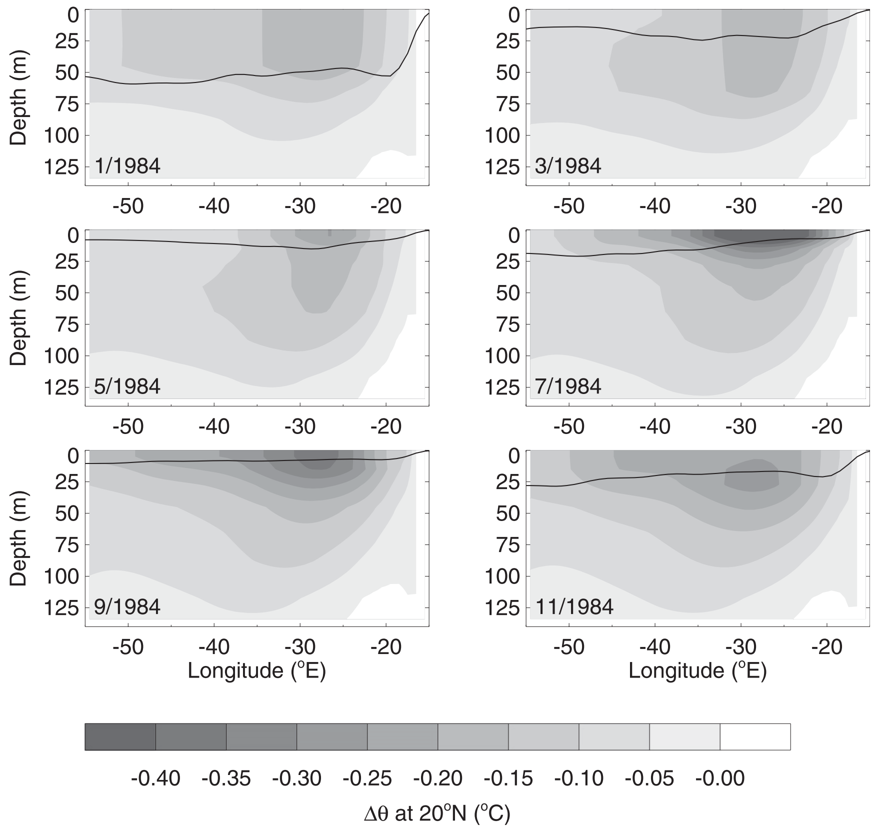

FIG. 12. The Δθ anomalies at depth along the 20°N transect during 1984. Shown are the monthly mean dust-forced change in potential temperature (Δθ) at depth (shaded contours) and the depth of the mixed layer from the model perturbed runs and based on the 0.125σ criteria.

minimum, and summertime forcing by anomalously high dust cover begins to further decrease Δθ within the ML.

As the ML remains shallow throughout July the magnitude of the Δθ anomalies are a maximum for the year; on the order of 0.5°C along the eastern half of the transect (Fig. 12). The eastern Δθ anomalies appear to mix down below the base of the very shallow summertime ML, to depths of 35 m, as evidenced by July Δθ anomalies that are below the base of the July ML but are larger in magnitude than the May Δθ anomalies. In September the magnitude of the Δθ anomalies within the ML are diminished, but the Δθ anomalies that are below the base of the ML are little changed from July.

In November, as the ML deepens, the surface anomalies are also mixed down (Fig. 12). Interestingly, in the November transect and in the vicinity of 30°W, the Δθ anomalies that had precipitated below the base of the ML during the summer months are of a magnitude greater than those Δθ anomalies seen within the ML, and the Δθ anomalies increase with depth from the surface to approximately 25 m. We note that for each plot in Fig. 12 the Δθ anomalies extend to depths of at least 125 m.

4. Discussion and conclusions

Using a 54-yr climatology of historical dust surface radiative forcing and an ocean general circulation model we estimated the physical response of the tropical and subtropical North Atlantic to anomalous African dust outbreaks on monthly to multidecadal time scales. Based on output from our model experiments, we conclude that over time the magnitude of the basin-averaged ΔT varies on interannual to multidecadal time scales (Figs. 8 and 9). Furthermore, on multidecadal time scales periods of warm and cool ΔT anomalies are in phase with—and of a magnitude comparable to—the AMO (Fig. 7). Periods of ΔT cool (warm) anomalies impose anomalous cyclonic (anticyclonic) circulation, and although the magnitude of the anomalous circulation was small, the change relative to the climatological currents was 5%–50% (Fig. 10). In addition, the depth of the composited dust-forced temperature change extends well below the base of the seasonal mixed layer, to depths of 125 m (Fig. 12).

In Mahowald et al. (2010) a composite map of dust forced changes in SST, similar to our Fig. 11 except for

10-yr composite differences, shows a region of cool anomalies ranging from 0.1° to 0.5°C extending southwestward from 15°N and 15°W. A 10-yr SST composite difference based on our data shows cool anomalies within this same range, although the anomalies largely extend westward from 15°N and not to the south (not shown). In Mahowald et al. (2010) dust-forced changes to SST are estimated using an atmospheric general circulation model coupled to a slab ocean; thus, the similarity between their and our results suggests that to first order the aerosol direct effect is the primary mechanism for aerosol-forced SST variability, and that both coupled effects and dynamical ocean processes may be neglected to first order. However, such an assumption may not hold on all time scales.

Additionally, in a paper published online after this manuscript was under consideration, Miller (2012) suggested that top-of-the-atmosphere radiative forcing by dust may be as important as the surface forcing component in determining the response of SSTs to anomalous atmospheric dust. However the relevance of top-of-the-atmosphere forcing strongly depends on the radiative properties of the aerosols and the thermal structure of the atmosphere.

Considering the limitation of our modeling approach, experiments with coupled models and eddy-resolving ocean models would be useful for assessing the importance of the aerosol direct effect, air–sea coupling, and ocean dynamics on various time scales. With regard to the ocean model, as eddy activity is thought to be weak in the region of strongest dust radiative forcing, and as our low-resolution model reproduces the ocean mean state fairly well, it is unlikely that increasing the model's resolution only will change our results dramatically.

African dust outbreaks are thought to be modulated by periods of drought in the Sahel region of West Africa (Prospero and Lamb 2003), and there is a strong influence of tropical SST on West African rainfall on decadal time scales (Giannini et al. 2003). Given that dust-forced ΔT anomalies are in phase with the AMO (Fig. 7) it is plausible that a coupled relationship among surface, atmospheric, and oceanic processes governs regional climate behavior, as is suggested in Evan et al. (2011). Given the disagreement in dust fluxes in climate models (Huneeus et al. 2010; Kok 2011), and uncertainty in future changes to source regions with global warming (Mahowald 2007), we suggest that quantifying the processes governing dust variability, and the role of dust in shaping past climate variability, is of paramount importance for estimating future change.

Acknowledgments. Funding for this work was provided by NOAA/CPO (NA10OAR4310136) to the University of Virginia and NA10OAR4310207 to University of Washington. We are grateful to two anonymous reviewers for their constructive comments on an earlier version of this manuscript.

REFERENCES

Adcroft, A., J.-M. Campin, P. Heimbach, C. Hill, and J. Marshall, cited 2002: MITgcm release 1 manual (online documentation). [Available online at http://mitgcm.org/sealion/online_documents/manual.pdf.]

Boyer, T. P., S. Levitus, H. E. Garcia, R. A. Locamini, C. Stephens, and J. Antonov, 2005: Objective analyses of annual, seasonal, and monthly temperature and salinity for the World Ocean on a 0.25° grid. *Int. J. Climatol.,* **25,** 931–945, doi:10.1002/joc.1173.

de Boyer Montégut, C., G. Madec, A. S. Fischer, A. Lazar, and D. Iudicone, 2004: Mixed layer depth over the global ocean: An examination of profile data and a profile-based climatology. *J. Geophys. Res.,* **109,** C12003, doi:10.1029/2004JC002378.

Deser, C., M. A. Alexander, and M. S. Timlin, 2003: Understanding the persistence of sea surface temperature anomalies in midlatitudes. *J. Climate,* **16,** 57–72.

Engelstaedter, S., I. Tegen, and R. Washington, 2006: North African dust emissions and transport. *Earth Sci. Rev.,* **79,** 73–100.

Evan, A. T., and S. Mukhopadhyay, 2010: African dust over the northern tropical Atlantic: 1955–2008. *J. Appl. Meteor. Climatol.,* **49,** 2213–2229.

——, and Coauthors, 2008: Ocean temperature forcing by aerosols across the Atlantic tropical cyclone development region. *Geochem. Geophys. Geosyst.,* **9,** Q05V04, doi:10.1029/2007GC001774.

——, D. J. Vimont, A. K. Heidinger, J. P. Kossin, and R. Bennartz, 2009: The role of aerosols in the evolution of tropical North Atlantic ocean temperature anomalies. *Science,* **324,** 778–781.

——, G. R. Foltz, D. Zhang, and D. J. Vimont, 2011: Influence of African dust on ocean–atmosphere variability in the tropical Atlantic. *Nat. Geosci.,* **4,** 762–765, doi:10.1038/ngeo1276.

Foltz, G. R., and M. J. McPhaden, 2006: The role of oceanic heat advection in the evolution of tropical North and South Atlantic SST anomalies. *J. Climate,* **19,** 6122–6138.

——, and ——, 2008a: Impact of Saharan dust on tropical North Atlantic SST. *J. Climate,* **21,** 5048–5060.

——, and ——, 2008b: Trends in Saharan dust and tropical Atlantic climate during 1980–2006. *Geophys. Res. Lett.,* **35,** L20706, doi:10.1029/2008GL035042.

Gent, P. R., and J. C. McWilliams, 1990: Isopycnal mixing in ocean circulation models. *J. Phys. Oceanogr.,* **20,** 150–155.

Giannini, A., R. Saravanan, and P. Chang, 2003: Oceanic forcing of Sahel rainfall on interannual to interdecadal time scales. *Science,* **302,** 1027–1030.

Huneeus, N., and Coauthors, 2010: Global dust model intercomparison in AeroCom phase I. *Atmos. Chem. Phys. Discuss.,* **10,** 23 781–23 864, doi:10.5194/acpd-10-23781-2010.

Husar, R. B., J. M. Prospero, and L. L. Stowe, 1997: Characterization of tropospheric aerosols over the oceans with the NOAA advanced very high resolution radiometer optical thickness operational product. *J. Geophys. Res.,* **102** (D14), 16 889–16 910.

Kalnay, E., and Coauthors, 1996: The NCEP/NCAR 40-Year Reanalysis Project. *Bull. Amer. Meteor. Soc.,* **77,** 437–471.

Kaufman, Y. J., I. Koren, L. A. Remer, D. Tanré, P. Ginoux, and S. Fan, 2005: Dust transport and deposition observed from the Terra-Moderate Resolution Imaging Spectroradiometer

(MODIS) spacecraft over the Atlantic Ocean. *J. Geophys. Res.,* **110,** D10S12, doi:10.1029/2003JD004436.

Kok, J. F., 2011: A scaling theory for the size distribution of emitted dust aerosols suggests climate models underestimate the size of the global dust cycle. *Proc. Natl. Acad. Sci. USA,* **108,** 1016–1021.

Large, W. G., J. C. McWilliams, and S. C. Doney, 1994: Oceanic vertical mixing: A review and a model with a nonlocal boundary layer parameterization. *Rev. Geophys.,* **32,** 363–403, doi:10.1029/94RG01872.

Mahowald, N. M., 2007: Anthropocene changes in desert area: Sensitivity to climate model predictions. *Geophys. Res. Lett.,* **34,** L18817, doi:10.1029/2007GL030472.

——, and Coauthors, 2010: Observed 20th century desert dust variability: Impact on climate and biogeochemistry. *Atmos. Chem. Phys.,* **10,** 10 875–10 893, doi:10.5194/acp-10-10875-2010.

Marshall, J., A. Adcroft, C. Hill, L. Perelman, and C. Heisey, 1997a: A finite volume, incompressible Navier–Stokes model for studies of the ocean on parallel computers. *J. Geophys. Res.,* **102** (C3), 5753–5766.

——, C. Hill, L. Perelman, and A. Adcroft, 1997b: Hydrostatic, quasi-hydrostatic, and nonhydrostatic ocean modeling. *J. Geophys. Res.,* **102,** 5733–5752.

Martínez Avellaneda, N. M., N. Serra, P. J. Minnett, and D. Stammer, 2010: Response of the eastern subtropical Atlantic SST to Saharan dust: A modeling and observational study. *J. Geophys. Res.,* **115,** C08015, doi:10.1029/2009JC005692.

Miller, R. L., 2012: Adjustment to radiative forcing in a simple coupled ocean–atmosphere model. *J. Climate,* in press.

——, and I. Tegen, 1998: Climate response to soil dust aerosols. *J. Climate,* **11,** 3247–3267.

Myhre, G., A. Grini, J. M. Haywood, F. Stordal, B. Chatenet, D. Tanré, J. K. Sundet, and I. S. A. Isaksen, 2003: Modeling the radiative impact of mineral dust during the Saharan Dust Experiment (SHADE) campaign. *J. Geophys. Res.,* **108,** 8579, doi:10.1029/2002JD002566.

Prospero, J. M., and P. J. Lamb, 2003: African droughts and dust transport to the Caribbean: Climate change implications. *Science,* **302,** 1024–1027.

Rayner, N. A., D. E. Parker, E. B. Horton, C. K. Folland, L. V. Alexander, D. P. Rowell, E. C. Kent, and A. Kaplan, 2003: Global analyses of sea surface temperature, sea ice, and night marine air temperature since the late nineteenth century. *J. Geophys. Res.,* **108,** 4407, doi:10.1029/2002JD002670.

Santer, B., and Coauthors, 2001: Accounting for the effects of volcanoes and ENSO in comparisons of modeled and observed temperature trends. *J. Geophys. Res.,* **106** (D22), 28 033–28 059.

Schollaert, S. E., and J. T. Merrill, 1998: Cooler sea surface west of the Sahara Desert correlated to dust events. *Geophys. Res. Lett.,* **25,** 3529–3532.

Trenberth, K. E., and D. J. Shea, 2006: Atlantic hurricanes and natural variability in 2005. *Geophys. Res. Lett.,* **33,** L12704, doi:10.1029/2006GL026894.

Wong, S., A. E. Dessler, N. M. Mahowald, P. R. Colarco, and A. da Silva, 2008: Long-term variability in Saharan dust transport and its link to North Atlantic sea surface temperature. *Geophys. Res. Lett.,* **35,** L07812, doi:10.1029/2007GL032297.

——, ——, ——, P. Yang, and Q. Feng, 2009: Maintenance of lower tropospheric temperature inversion in the Saharan air layer by dust and dry anomaly. *J. Climate,* **22,** 5149–5162.

Yoshioka, M., N. M. Mahowald, A. J. Conley, W. D. Collins, D. W. Fillmore, C. S. Zender, and D. B. Coleman, 2007: Impact of desert dust radiative forcing on Sahel precipitation: Relative importance of dust compared to sea surface temperature variations, vegetation changes, and greenhouse gas warming. *J. Climate,* **20,** 1445–1467.